Analysis and Design of Microwave Absorbers Combining Surface Wave Attenuation and Reflection Bandwidth Properties

Varsha Mishra, *Member, IEEE*, and Agostino Monorchio, *Fellow, IEEE*

***Abstract*—A new method is outlined in this manuscript to design an optimized microwave absorber (MA) achieving the desired level of reflection bandwidth (RBW) and surface wave attenuation (SWA). The proposed semianalytical two-dimensional dynamic method is best suited for the type of MAs consisting of either single-layer or multilayer impedance surfaces, such as resistive sheets and meta-materials. The proposed work contains the following two aims: 1) computation of the SWA in meta-material-based absorbers and 2) optimization of MA parameters for obtaining the desired level of SWA and RBW. To achieve the first aim, a complete mathematical explanation is outlined in detail, and further, to validate it, a particular example is implemented through which it is possible to simulate and analyze the structure via full-wave simulations. This proposed methodology is further integrated with the multiobjective optimization process of a genetic algorithm to achieve the second aim. Consequently, optimization of MA parameters is carried out and the desired level of outputs (i.e., RBW and SWA) is achieved. The proposed approach is explained by means of various examples of MAs and after detailed analysis, some competitive solutions are achieved. The proposed work can be widely applied in microwave frequency-based electronic devices to avoid surface electromagnetic wave coupling.**

***Index Terms*—Meta-materials, microwave absorbers (MAs), reflection bandwidth (RBW), surface waves attenuation.**

I. Introduction

In RECENT years, the use of wireless devices has enormously increased due to the introduction of the Internet of Things (IoTs) in wireless devices. However, to integrate IoTs in wireless devices for multiple different real-world applications, a wide frequency bandwidth (BW) is required. The wide BW requirement is being fulfilled using wireless devices of nanoscale. These devices are well-known as microwave integrated circuits (MICs) and have wide consumption in various commercial platforms. The MICs share the same substrate for various electronic/wireless devices that impose space constraints, which results in electromagnetic wave coupling (EMWC) [1], [2], [3]. The EMWC can result in various hazards in electronic devices due to crosstalk, such as an increase in temperature, fluctuation, and sudden interruption of closing of the ongoing operation.

In order to mitigate the EMWC effect, microwave absorbers (MAs) have been widely used between the devices [4], [5], [6], [7]. Initially, the MAs have been developed by using the lossy magnetic and dielectric materials [8], [9], [10], [11]. The absorption properties of the MAs, depend on both electrical parameters (e.g., permittivity, permeability, and particle morphology) and physical parameters (e.g., thickness of the sheet) of the material [11]. For the efficient development of MAs, various techniques, such as multilayering of lossy material [12], developing the composite materials [11], and coating of the resistive sheets (e.g., Salisbury Screen and Jaumann [13], [14]), circuit analog absorbers (CAAs) [10], [15], [16], and meta-materials [17], [18], [19] have been proposed. However, efficient implementation of these techniques requires a suitable optimization method or parametric analysis, according to the requirement and suitability of the methodology. Various optimization techniques, such as genetic algorithm (GA) [11], [15], [20], [21], particle swarm optimization (PSO) [22], [23], and artificial bee colony (ABC) [24] have been utilized in literature for obtaining the desired response based on the application.

The developed MAs are required to be applied in between the electronic device components of MICs to reduce the EMWC. The utilization of MAs between the MICs' components requires proper quantification of the surface wave coupling. The propagation constant of surface wave with respect to operating frequency, known as the dispersion diagram is analyzed to quantify the coupling. The dispersion diagram of EBG (electromagnetic band gap) structures [25], [26], [27], [28] can be easily analyzed by eigenmode solver of simulation software. However, complexity of the structure and narrow bandwidth are the drawbacks limiting the usage of the EBG. Moreover, analyzing the dispersion diagram of MAs is not possible by using the simulation software. To perform this task, various methodologies have been proposed to quantify the complex surface wave propagation constant in different kinds of MAs, such as single layered lossy media [29], [30], [31], dielectric layer coated with resistive sheet, [32], [33], and multilayering of lossless/lossy dielectric media [34], [35], [36]. Real and imaginary parts of complex propagation constant indicate the attenuation and propagation constants of surface wave,

Manuscript received 30 April 2023; revised 20 August 2023 and 13 October 2023; accepted 7 November 2023. This work was supported by the Italian Ministry of Education and Research (MUR) in the framework of the FoReLab and CrossLab projects of DII of the University of Pisa (Departments of Excellence). *(Corresponding author: Varsha Mishra.)*

Varsha Mishra and Agostino Monorchio are with the Department of Information Engineering, University of Pisa, 56126 Pisa, Italy, and also with the RaSS Lab of CNIT, 56124 Pisa, Italy (e-mail: varsha.mishra@ing.unipi.it; agostino.monorchio@unipi.it).

Color versions of one or more figures in this article are available at https://doi.org/10.1109/TEMC.2023.3339511.

Digital Object Identifier 10.1109/TEMC.2023.3339511

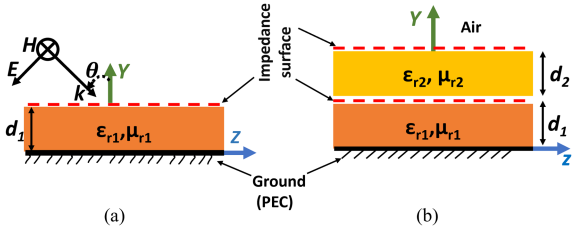

Fig. 1. Schematic of MAs. (a) Config-I: Grounded dielectric slab coated with infinitely thin resistive sheet^a or resistive patch FSS^b. (b) Config-II: Multilayering of dielectric slabs and thin resistive sheets^a or resistive patch FSS^b.

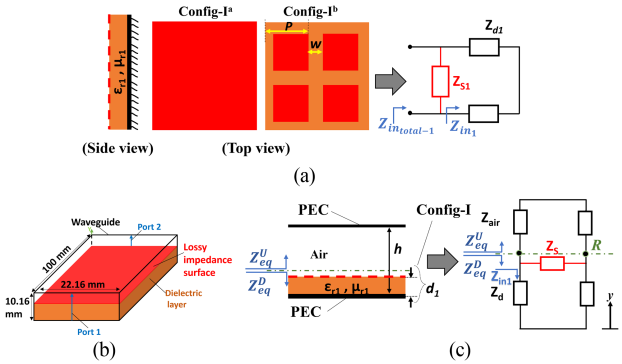

Fig. 2. (a) Schematic diagram and equivalent circuit of both open-ended Config-I^a and Config-I^b (side view and top view). (b) Schematic of waveguide setup simulated in an Ansys HFSS for validation. (c) The equivalent circuit of waveguide setup includes Config-I^a/Config-I^b.

respectively. Besides that, an approach, named as two-dimensional dynamic method (2D-DM), is presented in [37]. 2D-DM method is quite efficient in computing the surface wave attenuation (SWA) in lossless/lossy multilayered media, and single layer resistive sheet coated over a lossless dielectric layer. However, no such method has been reported for meta-materials-based microwave absorbers (MMAs). Meta-materials are considered one of the most utilized structures of modern times due to their wide BW and low profile characteristics. Hence, it is required to establish an efficient approach to analyze the complex nature of the surface wave propagation constant in such absorbers.

In this article, we outline a novel approach that evaluates the surface wave propagation constant of the meta-material-based absorber. Further, to reduce the EM coupling, it is desired to achieve the maximum possible values for reflection bandwidth RBW, and SWA in the same frequency band [30], [38]. Therefore, a new optimization technique is also proposed in this article, that optimizes the MAs to achieve the maximum possible values of RBW and SWA together in the desired frequency band. The rest of this article is organized as follows. Section II includes a detailed description of the proposed method and its validation. Section III explains an optimization process with resistive-sheet-based absorbers and also outlines an approach to achieve the desired level of RBW and SWA. Section IV analyzes and discusses the results outcomes obtained for the other examples of meta-material-based absorbers. Finally, Section V concludes this article.

II. Proposed Method: Explanation and Validation

In this section, a detailed description of the proposed methodology and its validation is explained by using a particular setup. The proposed methodology is explained in step-by-step manner, presenting the quantitative analysis for single-layer MAs, i.e., Config-I^a and Config-I^b. The schematics of the considered classical MAs are shown in Fig. 1(a). To further achieve more practical solutions, the proposed methodology is also implemented on complex structures made up of multilayering, as demonstrated in Fig. 1(b).

The proposed methodology utilizes a well-established theory of equivalent transmission line (Eq-TL) model and transverse resonance method (TRM) [1]. Both concepts are popularly explained in literature [10], [11], [12], [13], [14], [15], [18], [19], [20], [21], [31], [32], [33], [34], [35], [36], [37]. Therefore, we refrain to explain them in detail here. However, the necessary formulations with the concise theoretical background on Eq-TL and TRM are added in the subsequent subsection preceding the explanation of the proposed methodology.

A. Theoretical Background

1) Eq-TL Model: The Eq-TL model is described to compute the reflection coefficient (S_{11}) of the MAs. The schematics of the considered MAs are shown in Fig. 1. These structures have air on top and are grounded with metal on the bottom side. The mathematical computation of S_{11} is described under the normal incidence of EM wave for the TM polarization mode. The S_{11} of MAs can be computed by using the TL model, given as follows:

$$S_{11} = \frac{Z_{\text{in}_{\text{total-k}}} - Z_0}{Z_{\text{in}_{\text{total-k}}} + Z_0} \tag{1}$$

where Z_0 is the characteristic impedance of the air (i.e., $Z_0 = 377\,\Omega$), and $Z_{\text{in}_{\text{total-k}}}$ is the equivalent impedance of MA having number of coating as $k = 1, 2, 3..\text{m}$. The equivalent circuit of the single-layer MAs (e.g., Config-I^a and Config-I^b), utilized for the mathematical explanation, is shown in Fig. 2(a).

2) TRM: Another desired goal is obtaining SWA for the considered MAs. It is computed by implementing the transverse resonance equation on the considered examples. The TRM states that, at any point on the resonant line, the sum of equivalent impedances seen looking to either side must be zero [1], i.e.,

$$Z^D_{\text{eq}} + Z^U_{\text{eq}} = 0. \tag{2}$$

where Z^D_{eq} and Z^U_{eq} are the downward- and upward- impedance, respectively. A specific example, along with its equivalent circuit is shown in Fig. 2(b). In this example, Config-I^{a,b} is situated at $z = 0$ plane, and it is shielded with PEC at the height of $h - d_1$. Once defining the resonant line (R) on the circuit, Z^D_{eq} can be interpreted as $Z_{\text{in}_{\text{total}-1}}$, and Z^U_{eq} can be defined as an impedance of "air-slab" closed with PEC on top [see, Fig. 2(b)].

The proposed mathematical approach relies on utilizing both (1) and (2) for computing the RBW and SWA, respectively, since the total impedance of the considered MA, i.e., $Z_{\text{in}_{\text{total-k}}}$ is required to solve both (1) and (2). Therefore, it is imperative

to provide a circuit analysis approach to compute the $Z_{\text{in}_{\text{total-k}}}$ of all the considered MAs.

3) Equivalent Circuit Analysis: In this part, the mathematical computation of $Z_{\text{in}_{\text{total-k}}}$ for the considered MA is explained. Config-I^a and Config-I^b indicate the single-layer grounded dielectric slab (GDS) coated with a thin resistive sheet and resistive patch FSS, respectively. The schematic and the equivalent circuit of the single-layer MAs, i.e., Config-I^{a,b} are shown in Fig. 2(a). The MAs are surrounded by the air medium on top.

The impedance of GDS can be expressed by using the transmission line formula as [1]

$$Z_{\text{in1}} = j\frac{\gamma_{y1}}{\omega\varepsilon_0\varepsilon_{r1}}\tan(\gamma_{y1}d_1) \tag{3}$$

where $\omega = 2\pi f$ is the angular frequency and γ_{y1} is the propagation constant of EM wave traveling in the substrate having relative permittivity ε_{r1}, relative permeability μ_{r1}, and thickness d_1. The equivalent impedance of coatings, such as infinitely thin resistive sheet and resistive patch FSS is assumed as Z_{S1}. The impedance (Z_{S1}) is purely real in case of infinitely thin resistive sheet. However, using resistive patch FSS as a coating, Z_{S1} become complex in nature and can be represented as $Z_{S1} = R + j\omega L + 1/j\omega C$, where ω is the operating angular frequency, and R, L, and C represents the resistance, inductance, and capacitance, respectively. The value of R, L, and C parameters can be computed from the retrieval method described in [15] and [39]. The retrieval method is considered as the most easy and accurate one. For the known values of S_{11}, Z_0, and Z_{in1}, equivalent impedance of MA can be defined as

$$Z_{S1} = \frac{Z_0 Z_{\text{in1}}(1+S_{11})}{Z_{\text{in1}}(1-S_{11}) - Z_0(1+S_{11})} \tag{4}$$

where S_{11} is the reflection coefficient of the considered MA, which is obtained by using Ansys circuit simulation. The value of R, L, and C can be estimated by comparing the real and imaginary part of Z_{S1}, respectively. The value of R, L, and C are tuned in the circuit to obtain the S_{11}, which validates the results of 3-D simulation of Ansys HFSS. Knowing the resonance frequency $f_0 = 1/2\pi\sqrt{LC}$, imaginary part of the lossy surface can be reinterpreted as $\text{Imag}(Z_{S1}) = (\omega^2 - \omega_0^2)L/\omega$. The estimation of C here is possible by tuning the value of L. Similarly, formula for estimating the real part of impedance is $\text{Real}(Z_{S1}) = R = R_s(S/A)$, where S and A are the surface areas of the whole unit cell and patch, respectively, and R_s is the resistivity of the surface in (Ω/sq). After computing the Z_{S1} and Z_{in1}, the total equivalent impedance of the single-layer MAs (where $k = 1$), can be expressed as

$$Z_{\text{in}_{\text{total}-1}} = \frac{Z_{\text{in1}} Z_{S1}}{Z_{\text{in1}} + Z_{S1}}, \tag{5}$$

Further, for the multilayer absorber, such as Config-II^{a,b}, the equivalent impedance can be computed as

$$Z_{\text{in2}} = Z_2\frac{Z_{\text{load}} + Z_2\tanh(\gamma_{y2}d_2)}{Z_2 + Z_{\text{load}}\tanh(\gamma_{y2}d_2)} \tag{6}$$

where $Z_{\text{load}} = Z_{\text{in}_{\text{total}-1}}$ [already derived in (5)], Z_2 is the characteristic impedance of second dielectric layer, and Z_{S2} is the impedance of second layer of lossy-coating, and can be estimated by the Ansys circuit simulation. Finally, equivalent impedance of the Config-II^{a,b} can be computed as $Z_{\text{in}_{\text{total}-2}} = (Z_{\text{in2}}Z_{S2})/(Z_{\text{in2}} + Z_{S2})$. The aforesaid theoretical background is utilized in the subsequent subsection for the establishment of the proposed method.

B. Proposed Methodology and Its Validation

In this section, a specific setup is utilized for the mathematical explanation and its validation. The setup consists of single-layer MAs positioned inside a waveguide structure as shown in Fig. 2(b) and (c). The validation of the proposed methodology is extremely important, since it ensures the correct implementation of the formulas. For this purpose, both Config-I^a and Config-I^b are positioned sequentially on the lower surface of the waveguide. A setup is developed in such a way that the computation of the complex propagation constant by using simulation software is possible. The 3-D simulation setup, which includes a waveguide structure containing the MAs, is shown in Fig. 2(b). Indeed, HFSS provides the complex propagation constant of the guiding structure. This is possible only for cases where two ports can be defined, whereas it is not possible for open structures. For this reason, we verified the correctness of our approach with this specific setup, which provides the complete solution for the surface wave propagation with Ansys HFSS even in the presence of losses.

Moreover, the equivalent circuit of waveguide setup is shown in Fig. 2(c). A nonlinear characteristic is defined, considering the structure is infinite in the x–z plane and the waveguide consists of MAs at $z = 0$ plane. The equivalent circuit of the considered validation setup that includes Config-I^a/Config-I^b within the waveguide can be analyzed mathematically from (2). The ground planes situated at the top and bottom, are considered as a short circuit. The characteristic equation for the corresponding structure can be given as

$$F_{\text{TMmode}} \Rightarrow Z_{\text{air}}\tanh(\gamma_{y0}(h-d_1)) + Z_{\text{in}_{\text{total}-1}} = 0 \tag{7}$$

where the value of Z_{eq}^U and Z_{eq}^D in (2) are replaced by $Z_{\text{air}}\tanh(\gamma_{y0}(h-d_1))$ and $Z_{\text{in}_{\text{total}-1}}$ [see, (5)], respectively. Further, all the elements of (7) can be expressed through (3)–(5) as

$$Z_{\text{in}_{\text{total}-1}} = Z_{\text{in1}}||Z_{S1}, Z_{\text{in1}} = Z_{d1}\tanh(\gamma_{y1}d_1)$$

$$\gamma_{y0} = \sqrt{\gamma_0^2 - \gamma_z^2};\ \gamma_{y1} = \sqrt{\gamma_d^2 - \gamma_z^2}$$

$$Z_{\text{air}} = \frac{\gamma_{y0}}{w\varepsilon_0};\ Z_{d1} = \frac{\gamma_{y1}}{w\varepsilon_0\varepsilon_d};\ \gamma_0 = \sqrt{\mu_0\varepsilon_0}\ \&\ \gamma_d = \gamma_0\cdot\sqrt{\varepsilon_1}$$

where γ_z is the root of nonlinear characteristic (7). For the considered structure, root of the characteristic equation is complex i.e., $\gamma_z = \alpha_z + j\beta_z$, and therefore searched in a 2-D plane i.e., $\alpha_z - \beta_z$ plane. The term F_{TMmode} is utilized to represents (7) and can be called as converged function. To obtain the root with higher accuracy and efficiency, ideally F_{TMmode} must be zero. Therefore, the analysis includes the computation of the root along with its accuracy measure i.e., F_{TMmode}.

1) Computation of Roots for the Setup Having Config-I^a: In this part, roots of the nonlinear characteristic (7) for the setup of waveguide consisting of Config-I^a at $z = 0$ plane, is analyzed. The partially filled material consists of $\varepsilon_1 = 4$, $\mu_1 = 1$, and

TABLE I
COMPLEX PROPAGATION CONSTANT AND CONVERGED FUNCTION VALUE OF SHIELDED CONFIG-I^a: RESISTIVELY COATED-SHIELDED MULTILAYER STRUCTURE WITH $\varepsilon_1 = 4$, $\mu_1 = 1$, $d_1 = 3.01$ MM, $h = 10.16$ MM IN THE FREQUENCY RANGE FROM 8 TO 12 GHZ

No.	Lossless media			Rs=400 Ω/sq		
	Frequency (GHz)	$\beta_{z_{(R_s=0)}}$	F_{TMmode}	α_z	β_z	F_{TMmode}
1	8.0	199.60	2.00E-04	17.33	188.56	1.2E-02
2	9.0	228.74	5.70E-04	23.85	210.03	6.6E-03
3	10.0	260.25	6.30E-04	31.63	228.92	1.3E-02
4	11.0	294.84	7.40E-04	38.94	243.69	2.7E-02
5	12.0	332.99	6.40E-04	42.41	255.21	2.5E-02

$d_1 = 3.01$ mm. The overall height of the structure is $h = 10.16$ mm. The TM_0 mode in the frequency range from 8 to 12 GHz is analyzed. The real impedance of an infinitely thin resistive sheet is equivalent to the resistivity of the sheet i.e., $R_s = R$. A step-by-step procedure of computing the propagation constant (γ_z) for this example is as follows.

1) Assuming the considered MA is lossless i.e., $R_s = 0$, the obtained γ_z will be real and positive i.e., $\gamma_z = \beta_{z_{(R_s=0)}}$. In the lossless structure, range for searching the root(s) is $k_0 \leq \beta_{z_{(R_s=0)}} \leq \sqrt{\varepsilon_1\mu_1}k_0$. Knowing all the physical and electrical parameters of the structure, the value of both $\beta_{z_{(R_s=0)}}$ and F_{TMmode} are computed in the frequency range from 8 to 12 GHz, and listed in Table I. The value of F_{TMmode} is converged upto the order of 1e-4. This range of F_{TMmode} is acceptable considering sufficient accuracy measure for the computation of the root(s).
2) Now, R_s is considered as nonzero i.e., $R_s = 400\,\Omega$/Sq. In this case, at given parameter of structure, the γ_z become complex quantity, i.e., $\gamma_z = \alpha_z + j\beta_z$. Both the value of α_z and β_z must satisfy (7), in such a way that F_{TMmode} converged to zero. For searching complex root(s) in 2-D plane, the range of α_z & β_z are defined as follows:

$$\text{Limit 1}: \; -\Delta\alpha_z/2 \leq \alpha_z \leq \Delta\alpha_z/2 \tag{8}$$

$$\text{where} \;\; \Delta\alpha_z = W_1 k_0 \tag{9}$$

$$\text{Limit 2}: \; -[\beta_{z(R_s=0)} - \Delta\beta_z/2] \leq \beta_z \leq [\beta_{z(R_s=0)} + \Delta\beta_z/2] \tag{10}$$

$$\text{where} \;\; \Delta\beta_z = W_2\beta_{z(R_s=0)}. \tag{11}$$

The value of $\beta_{z(R_s=0)}$ is already obtained in the previous step. The weights W_1 and W_2 are employed to regulate the upper and lower limits of α_z and β_z, respectively. The converged function is achieved up to the order of 1e-2. The obtained converged function value and respective complex propagation constant are summarized in Table I. The weights are tuned according to the losses, and searching area is changed precisely to achieve the condition of optimum convergence. In case of $R_s = 400\,\Omega$/Sq, W_1 and W_2 both are tuned to 0.1. This tuning ability of W_1 and W_2 provide the dynamic area of $\alpha_z - \beta_z$ plane.

The aforementioned specific example of validation providing the roots with acceptable accuracy. Therefore, the roots of (7) are further computed by varying impedance of resistive sheet from 300 to 1000 Ω/Sq, and the frequency from 8.2 to 12.4 GHz.

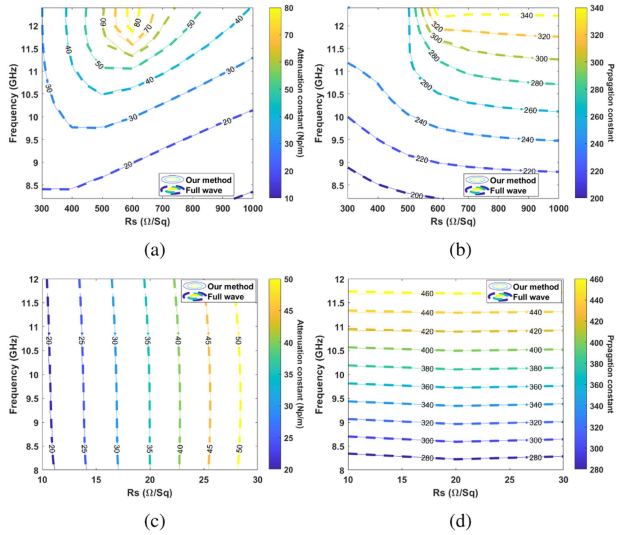

Fig. 3. Comparison between our method [i.e., (7)] and Ansys HFSS simulation (or full wave) at the TM_0 mode of (a) attenuation, and (b) propagation constant when Config-I^a is used as partially filled material where the resistive impedance and frequency are varied from 300 to 1000 Ω/Sq, and 8.2 to 12.4 GHz, respectively. (c) Attenuation and (d) propagation constant when Config-I^b is used as partially filled material where the resistive impedance and frequency are varied from 10 to 30 Ω/Sq, and from 8.2 to 12.4 GHz, respectively.

The contour plots of attenuation- and propagation- constant with respect to resistive impedance and frequency are plotted in Fig. 3(a) and (b), respectively. It is observed here that considering the resistance as a constant, attenuation increases with increase in operating frequency.

In this part, roots are computed by using the 2D-DM. The 2D-DM method was initially introduced in our previous work of [37] and shown efficient in computing the roots with accuracy and rapidity due to its dynamic behavior. However, in this conventional 2D-DM method, the analysis of the roots was limited to multilayered lossy materials and lossless dielectric material coated with thin resistive sheet (but only single layer). With the conventional 2D-DM method, it was not possible to characterize the surface wave propagation constant of the most popular type of MA structures i.e., meta-material based MA designs. Therefore, the conventional 2D-DM is modified here, to make it suitable for meta-material-based MA. The method is explained in the subsequent subsection where the setup containing the coating of meta-material (i.e., Config-I^b) is analyzed.

2) Computation of Roots for the Setup Having Config-I^b: In this part, the root(s) of (7) referring to the waveguide structure

TABLE II
COMPLEX PROPAGATION CONSTANT AND CONVERGED FUNCTION VALUE OF SHIELDED CONFIG-I^b: RESISTIVE PATCH COATED STRUCTURE WITH $\varepsilon_1 = 4$, $\mu_1 = 1$, $d_1 = 1.5$ MM, $h = 10.16$ MM IN THE FREQUENCY RANGE FROM 8 TO 12 GHZ

No.	Lossless media			$R_s = 10\ \Omega$/Sq		
	Frequency (GHz)	$\beta_{z_{(R=0)}}$	F_{TMmode}	α_z	β_z	F_{TMmode}
1	8.0	265.19	3.07E-03	18.27	266.22	6.72E-02
2	9.0	331.81	1.06E-03	18.64	332.86	5.31E-02
3	10.0	373.31	0.62E-03	18.75	374.26	2.91E-02
4	11.0	419.12	3.81E-03	18.95	419.89	6.79E-02
5	12.0	460.33	1.81E-03	19.24	460.89	6.87E-02

containing Config-I^b is explained, its schematic and equivalent circuit are described in Fig. 2(a)–(c). In this analysis, lossy surface is resistive patch FSS. Hence, the impedance of the coating in Config-I^b is complex as well as frequency dependent, whereas, in Config-I^a, Z_{S1} was purely resistive and constant with respect to the frequency. A step-by-step process to compute the root(s) of (7) is described as follows.

1) First, the impedance of resistive patch FSS (Z_{S1}) is analyzed by using the theory of equivalent circuit analysis, as explained in Section II.A.3. All elements of the Z_{S1}, such as resistance (R), capacitance (C), and inductance (L) are computed for the known physical parameters of Config-I^b. Selecting the substrate layer of $\varepsilon_1 = 4$, $\mu_1 = 1$ $d_1 = 1.5$ mm, and resistive patch FSS of periodicity (P) = 10 mm, Gap (w) = 2.5 mm, and resistivity (R_s) = 10 Ω/Sq, the value of R, L, and C are obtained as $R = 21.62\,\Omega$, $L = 0.622$ nH, and $C = 164.12$ fF, respectively. Once the equivalent value of R, L, and C are computed, the value of $Z_{\text{in}_{\text{total}-1}}$ can also be evaluated by inserting the value of $Z_{\text{in}1}$ and Z_{S1} in (5). Finally, $Z_{\text{in}_{\text{total}-1}}$ is put in to (7), and we computed the root(s) in the $\alpha_z - \beta_z$ plane.
2) For computing the root(s), first the structure has to assume lossless i.e., $R_s = 0$, and the 1-D search of the roots is conducted in the following range: $k_0 \leq \beta_{z_{(R_s=0)}} \leq \sqrt{\varepsilon_1\mu_1}k_0$. The value of F_{TMmode} is satisfactorily converged up to the order of 1e-3. The obtained propagation constants and converged function values are summarized in Table II.
3) In the final step, for the known value of $\beta_{z_{R_s=0}}$, complex propagation constant is computed in 2-D $\alpha_z - \beta_z$ plane, by using (8)–(11). In this case, the tuning parameters, such as W_1 and W_2 are set to 0.05 and 0.01, respectively. The value α_z, β_z and corresponding F_{TMmode} are summarized in Table II. The value of F_{TMmode} for this case is converged up to order of 1e-2.

Further, the obtained values of attenuation and propagation constants are plotted in Fig. 3(c)–(d) by varying the resistivity of patch FSS from 10 to 30 Ω/Sq and the frequency range from 8 to 12 GHz. The aforesaid range of resistivity is chosen because it provide good absorption properties of Config-I^b when used that particular range. It is evident that the proposed method to compute the SWA of meta-material based MA designs, includes both analytical and numerical method. Therefore, the proposed method is named here as "semianalytical 2D-DM". Likewise, more complex meta-material based MA designs can be solved with the proposed semianalytical 2D-DM.

3) 3-D Simulation Setup for the Validation: The waveguide structure contains the Config-I^{a,b} inside it at $z = 0$ plane [see, in Fig. 2(b)]. For validation of the proposed approach, the specific waveguide is simulated in the Ansys HFSS software. A partially filled X-band waveguide with length = 100 mm, width = 22.16 mm, and height = 10.16 mm, is considered. Both the ends of the waveguide, i.e., at $z = 0$ mm and $z = 100$ mm, are excited by wave port. The PMC boundary is applied at both $x = 0$ mm and $x = 22.86$ mm plane, whereas the PEC boundary at both $y = 0$ mm and $y = 10.16$ mm plane. The partially filled dielectric material is coated with lossy impedance surfaces. A 3-D model with details of size-, boundary conditions-, excitation- of the waveguide, and material characteristics of filled material is shown in Fig. 2(b).

Consequently, the complex propagation constant at the TM_0 mode is obtained. Comparison between mathematical model [see (7)] and Full-wave simulation at the TM_0 mode is shown in Fig. 3(a)–(d). The contour plot of attenuation and propagation constants are shown by varying both resistivity (Ω/Sq) and frequency (GHz). Contour plots of both α_z and β_z are plotted with respect to the resistivity of the impedance surfaces, i.e., infinitely coated thin resistive sheet [see, Fig. 3(a) and (b)] and periodic resistive patch FSS [see, Fig. 3(c) and (d)], respectively. It is evident from the results of both type of setups that the comparison of the proposed methodology with full-wave simulation is very good.

Results obtained from the proposed methodology show that the real part of propagation constant (i.e., attenuation constants of surface wave) depends on the parameters of Config-I^{a,b}, such as thickness of the dielectric substrate, permittivity, and permeability, impedance of the resistive sheet, and parameters of the FSS (periodicity and gap between patches). In order to achieve the maximum attenuation for reducing the surface EM wave as well as to achieve the maximum RBW, a systematic approach is needed to be developed. Given this aim, parameters of MA are optimized with the goal to achieve desired RBW and SWA by using an optimizing tool. Therefore, in the next section, the optimization process is carried out to achieve the desired solution with an easy, accurate, and efficient solving process.

III. ANALYSIS OF RESISTIVE SHEET BASED MAS

In this section, GA optimization tool is integrated with the proposed semianalytical 2D-DM to obtain the optimized solutions for the desired multiple objectives, such as RBW and SWA. Mainly, (1) and (2) are used to compute RBW and SWA,

TABLE III
LIST OF OPTIMIZING PARAMETERS FOR THE CONFIG-I^a

Parameters	Range	
	Min value	Max Value
ε_{r_1}	2.0	10.0
Z_{S1}	200.0 Ω	500.0 Ω
d_1	4.0 mm	10.0 mm

respectively. The proposed optimization approach is explained by using single layer and multilayer resistive sheet-based MAs, i.e., Config-I^a and Config-II^a. Considered MAs have infinite air medium on the top and are grounded at the bottom side [see, Fig. 1(a) and (b)]. The characterization of MAs is carried out in the frequency range from 1 to 18 GHz, under the following steps:

A. Step 1—Population Vector

Population vector is a set of chromosomes representing the parameters of the MA. In this case, a set of population vector consists of permittivity (ε_r), impedance of coated surface (Z_S), and thickness of the substrate (d). The parameters of MA are chromosomes of the population vector, which is represented as

$$X = [\varepsilon_{r_i}, Z_{S_i}, d_i] \tag{12}$$

where $i = 1, 2, 3, \ldots, N$ is the number of substrate layers. Hence, for the Config-I, (i.e., $N = 1$), the number of parameters is three, and for Config-II, (i.e., $N = 2$), the number of parameters is six. The parameters get evolved with each successive generation of GA optimization within a provided range of value of chromosomes. Therefore, the minimum and maximum values of these parameters needed to be defined. For example, the range of parameters for Config-I^a are summarized in Table III.

B. Step 2—Development of Cost Function

The development of cost function is carried out to minimize the error between desired output and computed output. Initially, user defines the outputs such as, $f_{o_{\text{Goal}}}$, RBW_{Goal}, and SWA_{Goal} at the initial stage. Afterwards, computed outputs are being converged to desired output by minimizing the following cost-function:

Cost function-1*:* The f_o is the minimum operating frequency at which the reflection coefficient becomes -10 dB. Hence, The following cost function is defined to calculate the difference between desired and computed reference operating frequency:

$$\text{CF}_1 = |(f_{o_{\text{Goal}}} - f_{o_{\text{Comp}}})| \tag{13}$$

where $f_{o_{\text{Goal}}}$ and $f_{o_{\text{Comp}}}$ are the reference operating frequencies of the desired output and computed output, respectively. The cost function is minimizing the desired reference frequency point through which RBW and SWA are computed.

Cost function-2*:* Once reference operating frequency (f_o) is computed, $\text{RBW}_{-5/-10\,\text{dB}}$ is calculated from the available S_{11}. An absolute error is computed between the desired and computed bandwidth of reflection coefficient (RBW) by using the following cost function:

$$\text{CF}_2 = |(\text{RBW}_{\text{Goal}} - \text{RBW}_{\text{Comp}})| \tag{14}$$

where RBW_{Goal} and RBW_{Comp} are the desired and computed RBWs, respectively.

Cost function-3*:* Similarly, the following cost function is developed to obtain the desired goal of SWA:

$$\text{CF}_3 = |(\text{SWA}_{\text{Goal}} - \text{SWA}_{\text{Comp}})| \tag{15}$$

where SWA_{Goal} and SWA_{Comp} are the desired output and computed output, respectively. $\text{SWA} = \frac{1}{K}\sum_{K=1}^{K} \alpha_z$, where α_z is the SWA constant at any single frequency point and K is the number of frequency points. For example, if maximum SWA is aimed greater than 10 Np/m, it means that the mean value of the attenuation constant (α_z) over considered frequency range is 10 Np/m. So that two antennas can be placed in a single PCB with minimum possible distance without any surface wave coupling. Hence, SWA_{Goal} is the mean value of the attenuation over considered frequency range, which is chosen as minimum 10 Np/m. The maximum of SWA is obtained by minimizing the $[\text{CF}_3(X)]^{-1}$.

The desired RBW and SWA in the defined frequency range are implemented by minimizing the overall fitness-function (FF_T), which is expressed as

$$\text{FF}_T = [\text{CF}_1(X), \text{CF}_2(X), [\text{CF}_3(X)]^{-1}]. \tag{16}$$

C. Step 3—Optimization and Postprocessing

The optimization of the parameters of MA is explained with various statistical results. Initially, the GA optimization is conducted by using the example of Config-I^a. The parameters of Config-I^a, such as ε_{r1}, Z_{S1}, and d_1 [see, (12)] are optimized for the following desired output: 5 GHz of "-10 dB RBW" ($\text{RBW}_{-10\,\text{dB}}$), SWA $\geq$ 10 Np/m, and $f_{o_{\text{Goal}}} = 5$ GHz. The fitness-function [see, (16)] is minimized for the desired output under the defined range of the optimizing parameters [see, Table III]. It states that the obtained solution may or may not the same in every independent run due to the inherent stochastic nature of GA [20]. Even though it has limitation, the GA is one of the reliable approaches to use in the condition despite a consistent form of solution that may or may not be obtained, as seen in [11], [15], [20], [21]. Although, we have already taken care of this point in our paper, and to avoid uncertainties in GA outcomes, selection of the solutions is based on statistical results. The analyzed statistical results of GA optimization are presented in Fig. 4(a)–(d). The fitness function with respect to generation is plotted to represent five independent runs as shown in Fig. 4(a). The similar trend is observed in all the cases that the value of the fitness function in each independent run reaches the minimum saturation level after approximately 60–75 generations. It is evident that before reaching to the minimum value of fitness function, the plot of fitness function versus generation is following nondeterministic path in every independent run. The nondeterministic behavior may occur due to random selection of initial population and changing of the parameters of GA, such as selection, mutation, crossover, and generation, etc. The GA optimization is conducted in *gamultiobj* tool of @MATLAB. However, the value of each independent run reaches to the minimum fitness function after approximately 60–75 generations [see, Fig. 4(a)]. Therefore, a maximum number of generations

TABLE IV
OPTIMIZED PARAMETERS OF CONFIG-I^a ABSORBERS, AT THE DESIRED OUTPUT OF $f_{o_{\text{GOAL}}}$, RBW, AND SWA

S. No.	Optimized parameters			Computed Outputs		
	Desired outputs-I: $f_{o_{\text{Goal}}}$ = 5 GHz, $RBW_{-5dB_{\text{Goal}}}$ = 5 GHz, and $SWA_{Goal} \geq$ 10 Np/m.					
	ε_r	$Z_S(\Omega)$	d (mm)	$f_{o_{\text{Comp}}}$ (GHz)	RBW_{Comp} (GHz)	SWA_{Comp} (Np/m)
1.	5.23	338.44	4.30	4.96	5.4 (4.96-10.36)	27.22
2.	4.71	341.76	4.62	4.72	5.52 (4.72-10.24)	24.27
3.	6.68	265.12	3.83	4.96 RBW	5.28 (4.96-10.24)	32.91
	Desired outputs-II: $f_{o_{\text{Goal}}}$ = 5 GHz, $RBW_{-10dB_{\text{Goal}}}$ = 5 GHz, and SWA $_{\text{Goal}} \geq$ 10 Np/m.					
4.	**2.01**	**301.00**	**5.6**	**6.63**	**5.47 (6.63-12.10)**	**12.69**
5.	2.00	265.52	6.0	6.41	4.92(6.41-11.32)	13.52
6.	2.06	279.83	5.8	6.40	5.16(6.4-11.56)	13.78

The bold values highlight the solutions which are plotted in Figure 5.

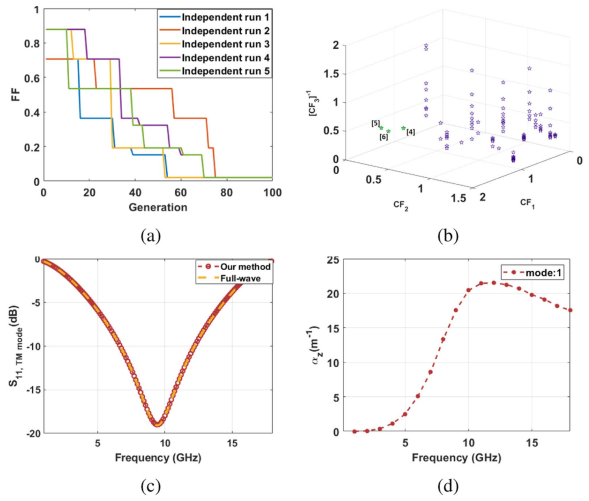

Fig. 4. (a) Fitness function versus generation of five independent runs, and (b) 3D Pareto plot shows the trade-off between CF_1, CF_2, and $[CF_3]^{-1}$. For the desired outputs, i.e., $f_{o_{\text{Goal}}}$ = 5 GHz, $\text{RBW}_{-10\,\text{dB}}$ = 5 GHz, and SWA $\geq$10 Np/m, three trade-off solutions are highlighted as *green stars*. Their corresponding parameters are listed in Table IV. The frequency dependent (c) reflection coefficient (S_{11} in dB), and (d) SWA (α_z) are computed outputs of GA optimization correspond to solution no. "4" [see, Table IV]. Their optimized parameters are $\varepsilon_r = 2.01$, $\mu = 1$, $Z_{S1} = 301\ \Omega$, and $d = 5.6$ mm.

is chosen as 100. Moreover, to optimize the considered MAs, the following key parameters of GA are used: A population size of 100, a "*tournament*" selection function, an "*adaptive feasible*" mutation function, a "*two-point*" crossover function, a "*fgoalattain*" hybrid function, and the default mutation and crossover probabilities. Moreover, the pareto-plot is shown in Fig. 4(b) for single independent run. It is a graphical representation, which shows the tradeoff between all the elements of fitness function [see, (16)]. The solutions listed in Table IV with indices "4," "5," and "6" are marked as "*green stars*" (for the proper visualization), representing the minimum trade-off between all three cost-functions. For the desired output of Config-I^a, the solutions are obtained and listed in Table IV with indices "4," "5," and "6," along with the obtained and desired outputs. Additionally, the obtained solutions of computed output i.e., RBW and SWA, are verified by plotting the frequency dependent reflection coefficient and SWA for the optimized parameters. The following optimized parameters $\varepsilon_{r1} = 2.01$, $\mu_{r1} = 1$, $Z_{S1} = 301\,\Omega$, and $d_1 = 5.6$ mm, correspond to the solution number "4" as listed in Table IV. Using these parameters, reflection properties (S_{11}) and attenuation constant (α_z) are plotted with respect to the frequency range from 1 to 18 GHz as shown in Fig. 4(c) and (d), respectively. It is observed that $\text{RBW}_{-10\,\text{dB}}$ is 5.47 GHz (from 6.63 GHz to 12.1 GHz) and SWA is 12.69 Np/m. The validation of the reflection coefficient with Ansys HFSS simulation is also represented in Fig. 4(c). It is evident that the proposed mathematical model can find the solutions with minimum cost function for the desired RBW and SWA in the defined frequency band.

In post processing, the efficiency of the proposed mathematical model is analyzed by optimizing the parameters for more different set of desired goals. This indicates the efficiency and capability of the method for providing multiple solutions with respect to different desired goals/outputs, which may fit to different applications. The desired outputs for Config-I^a is chosen as follows.

1) *Desired output-I:* $f_{o_{\text{Goal}}}$ = 5 GHz, 5 GHz of "−5 dB RBW" ($\text{RBW}_{-5\text{dB}}$), and $SWA \geq$10 Np/m.
2) *Desired output-II:* $f_{o_{Goal}}$ = 5 GHz, 5 GHz of "−10 dB RBW" ($RBW_{-10\,dB}$), and $SWA \geq$10 Np/m.

At the abovementioned desired goals, parameters of MA are optimized. The obtained optimized solutions, and the computed outputs are shown in Table IV. It is observed that proposed methodology can compute the outputs, which are close to their respective desired outputs, and provide the optimized parameters accordingly. It is evident that by using proposed methodology, parameters of MAs can be optimized at desired level of RBW and SWA.

Moreover, the Config-II^a consists of the following parameters: thickness (d_1, d_2), impedance (Z_{S_1}, Z_{S_2}), and permittivity (ε_{r_1}, ε_{r_2}) of layer 1 and layer 2, respectively. The parameters are optimized for desired level of RBW and SWA. The optimization is carried out for the following two categories of outputs: I. $f_{o_{\text{Goal}}}$ = 5 GHz, $\text{RBW}_{-5\,\text{dB}}$ = 10 GHz, and SWA $\geq$ 10 Np/m; II. $f_{o_{\text{Goal}}}$ = 5 GHz, $\text{RBW}_{-10\,\text{dB}}$ = 10 GHz, and SWA $\geq$ 2 Np/m. The obtained optimized parameters are summarized in Table V. Finally, solution no. 4 of Config-I^a [see, Table IV] and solution no. 6 of Config-II^a [see, Table V] are chosen, respectively, and frequency dependent reflection coefficient, SWA, and normalized propagation constant are plotted in the frequency range from 1 to 18 GHz, as shown in Fig. 5(a)–(c), respectively.

TABLE V
OPTIMIZED PARAMETERS OF CONFIG-II^a ABSORBERS, AT THE DESIRED OUTPUT OF $f_{o_{\text{GOAL}}}$, RBW, AND SWA

S.No.	Optimized parameters						Computed outputs		
	Desired outputs-I: $f_{o\,\text{Goal}} = 5$ GHz, $RBW_{-5dB\,\text{Goal}} = 10$ GHz, and $\text{SWA}_{\text{Goal}} \geq 10$ Np/m.								
	ε_{r1}	ε_{r2}	Z_{S1} (Ω)	Z_{S2} (Ω)	d_1 (mm)	d_2 (mm)	f_{Comp} (GHz)	RBW_{Comp} (GHz)	SWA_{Comp} (Np/m)
1.	3.34	3.12	393.47	443.19	2.44	2.39	5.08	9.96 (5.08-15.04)	22.82
2.	3.43	2.91	412.08	485.12	2.51	2.48	5.08	9.96(5.08-15.04)	21.59
3.	3.30	2.91	426.2	456.23	2.52	2.41	5.08	9.84(5.08-14.92)	21.79
	Desired outputs-II: $f_{o\,\text{Goal}} = 5$ GHz, $RBW_{-10dB\,\text{Goal}} = 10$ GHz, and $\text{SWA}_{\text{Goal}} \geq 2$ Np/m.								
4.	1.19	1.53	235.03	459.89	3.30	4.36	5.82	10.06 (5.82-15.88)	3.02
5.	1.14	1.69	225.98	511.42	4.67	5.18	4.60	10.44(4.6-15.04)	3.24
6.	**1.54**	**2.21**	**217.88**	**608.73**	**3.49**	**3.34**	**6.16**	**9.84(6.16-16)**	**6.85**

The bold values highlight the solutions which are plotted in Figure 5.

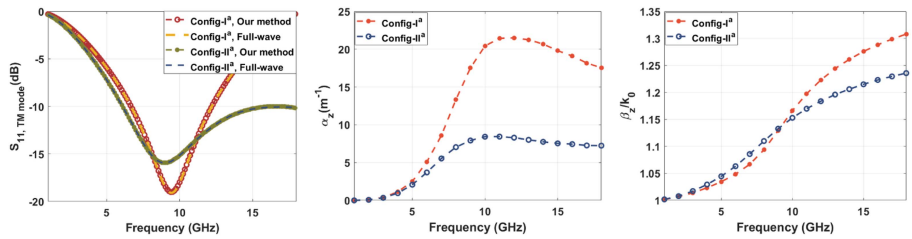

(a) (b) (c)

Fig. 5. Graphical solution of (a) reflection coefficient, (b) attenuation constant, and (c) Normalized propagation constant for Config-I^a (solution number 4 in Table IV) and Config-II^a (solution number 6 in Table V) having impedance surface of infinitely thin resistive sheet.

Moreover, the minimum theoretical limit of thickness is proposed by Rozanov et al., [40] to analyze the efficacy of the proposed design. Therefore, Rozanov thickness limit (RTL) is evaluated here as an additional parameter to analyze the efficiency of proposed method. The obtained absorber designs with solution no. 4 of Config-I^a [see, Table IV] and solution no. 6 of Config-II^a [see, Table V] are compared against the minimum RTL calculated according to the well-known formula given in [40]. For Config-I^a, Rozanov thickness and computed thickness are 4.5 and 5.4 mm, respectively. Similarly, Rozanov thickness and computed thickness for Config-II^a, are 5.6 and 6.1 mm, respectively. It is evident that proposed mathematical model is providing the unique and efficient solutions, which are important for the application that requires desired level of SWA and RBW.

IV. ANALYSIS OF META-MATERIAL BASED MAS

In this section, desired solution for the meta-material-based MAs such as Config-I^b and Config-II^b are evaluated using the proposed methodology, which is established and validated in Section II. The solutions are obtained by optimizing the parameters of Config-I^b and Config-II^b. First, the solutions of the Config-I^b are computed for the following desired outputs:

1) *Desired Output-I:* $f_{o_{\text{Goal}}} = 10$ GHz, $\text{RBW}_{-5\,\text{dB}} = 10$ GHz, and $\text{SWA} \geq 10$ Np/m and,
2) *Desired Output-II:* $f_{o_{\text{Goal}}} = 10$ GHz, $\text{RBW}_{-10\,\text{dB}} = 10$ GHz, and $\text{SWA} \geq 10$ Np/m.

Steps of obtaining the desired outputs and their optimized parameters, are summarized in brief as follows:

1) Resistivity of the patch (R_s), thickness of the dielectric (d_1), and gap between the patch (w) are chosen to be optimized while permittivity (ε_{r1}), permeability (μ_{r1}) of the substrate, and periodicity of the patch (P) are predefined as 2.0, 1.0, and 10 mm, respectively.
2) To obtain desired RBW, parameters of Config-I^b, i.e., R_s, d_1, and w, are optimized using CF_1, and CF_2 [see, (13) and (14)].
3) For the optimized value of R_s, d_1, and w, equivalent value of R, L, and C are retrieved. Further, by using CF_3 [see, (15)], maximum of SWA is analyzed.

All the desired solutions of the Config-I^b are obtained for the desired output-I and II as summarized in Table VI . One of the obtained solutions from the desired output-II of the Config-I^b that has the parameters $R_s = 40\,\Omega$/Sq, $d_1 = 3$ mm, and $w = 2.5$ mm is plotted in Fig. 6 . The equivalent value of R, L, and C of the resistive patch FSS are obtained as $R = 180\,\Omega$, $L = 1.1539$ nH, $C = 42.64$ fF, respectively. Moreover, the Config-II^b is also analyzed for the following desired output: $f_{o_{\text{Goal}}} = 5$ GHz, $\text{RBW}_{-10\,\text{dB}} = 10$ GHz, and $\text{SWA} \geq 10$ Np/m. Config-II^b consists of multilayering of dielectric layer and resistive patch FSS, alternatively. Permittivity and permeability of the layer 1 and 2 are $\varepsilon_{r1} = 2$, $\varepsilon_{r2} = 1.7$, $\mu_{r1} = 1$, and $\mu_{r2} = 1$, respectively. To obtain the optimized solution of the Config-II^b, elements of population vector are selected as R_{s1}, R_{s1}, d_1, d_2, w_1, and w_2. The optimized solutions for the desired output are optimized as $R_{s1} = 40\,\Omega$/Sq, $R_{s2} = 10\,\Omega$/Sq, $d_1 = d_2 = 2$ mm, $w_1 = 1.5$, $w_2 = 3$ mm. The equivalent values of resistive patch FSS are obtained as: $R_1 = 89\,\Omega$; $L_1 = 0.8$ nH; $C_1 = 75$ fF; $R_2 = 62.5\,\Omega$; $L_2 = 1$ nH; $C_2 = 28$ fF. Obtained output is $\text{RBW}_{-10\,\text{dB}} = 9.4$ GHz (from 8.2 to 17.6 GHz) and $\text{SWA} = 40$ Np/m. The total optimized thickness of Config-I^b and Config-II^b are 3 and 4 mm, respectively, which are only 0.08λ and 0.11λ of the lowest frequency. However, the RTLs for Config-I^b and Config-II^b are 2.4 and 3.1 mm, respectively. The additional evaluation of the thickness parameter of the obtained

TABLE VI
OPTIMIZED PARAMETERS OF CONFIG-I^b ABSORBER, AT THE DESIRED OUTPUT OF $f_{o_{\text{GOAL}}}$, RBW, AND SWA

Solution no.	Optimized outputs			RBW	Computed parameters	
	Desired outputs-I: $f_{o\,\text{Goal}} = 10$ GHz,			$-5dB_{\text{Goal}} = 10$ GHz, and $SWA_{\text{Goal}} \geq 10$ Np/m.		
	$R_S(\Omega/Sq)$	d (mm)	w (mm)	$f_{o\,\text{Comp}}$ (GHz)	RBW_{Comp} (GHz)	SWA_{Comp}(Np/m)
1.	35.0	3.0	2.0	7.9	10.1 (7.9-18)	41.00
2.	35.0	3.0	2.5	8.9	9.1(8.9-18)	37.73
3.	40.0	2.0	2.0	9.4	8.6(9.4-18)	98.00
	Desired outputs-II: $f_{o\,\text{Goal}} = 10$ GHz,			RBW $_{-10dB_{\text{Goal}}} = 10$ GHz, and $SWA_{\text{Goal}} \geq 10$ Np/m.		
4.	40.0	2.5	2.0	9.33	4.76(9.33-14.09)	67.00
5.	40.0	2.5	2.5	11.20	6.8(11.2-18)	60.00
6.	40.0	3.0	2.5	10.26	5.02(10.26-15.28)	41.00

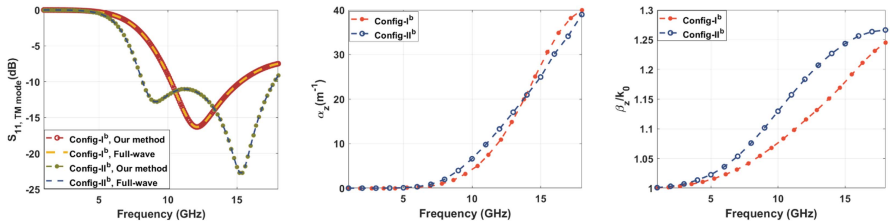

(a) (b) (c)

Fig. 6. Graphical solution of (a) reflection coefficient, (b) attenuation constant, and (c) Normalized propagation constant for Config-I^b and Config-II^b having impedance surface of resistive patch. Config-I^b with resistive patch achieved solution as $Rs = 40\,\Omega$/Sq, thickness of dielectric $(d_1) = 3$ mm, and gap between patch $(w) = 2.5$ mm, permittivity $(\varepsilon_{r1}) = 2.0$, permeability $(\mu_{r1}) = 1$, and periodicity of the patch $(P) = 10$ mm, and equivalent R-L-C of $R = 180\,\omega$, $L = 1.1539$ nH, $C = 42.64$ fF; Config-II^b with two layers of dielectric layer and resistive patch FSS alternately. Layer 1: $\varepsilon_{r1} = 2$, $\mu_{r1} = 1$, $d_1 = 2$ mm, $R_1 = 89\,\Omega$, $L1 = 0.8$ nH $C1 = 75$ fF (Patch size: Periodicity $(P) = 10$ mm, Gap $(w) = 1.5$ mm); Layer 2: $\varepsilon_{r2} = 1.7$, $\mu_{r2} = 1$, $d_2 = 2$ mm, $R_2 = 62.5$, $L_2 = 1$ nH $C_2 = 28$ fF (Patch size: Periodicity $(P) = 10$ mm, Gap $(w) = 3$ mm.

MA'design is carried out by using the RTL, to identify the physical design efficiency from the engineering point of view.

V. CONCLUSION

We have proposed a "semianalytical 2D-DM" to compute the SWA of meta-material based MAs. The methodology is validated by designing a specific waveguide structure in Ansys HFSS simulation software. Further, the proposed methodology is integrated with GA optimization tool, to compute the desired level of RBW and SWA properties in the microwave absorbing structures. For the performance evaluation, various MA examples possessing single or multiple substrate layers coated with either resistive sheet or resistive patch FSS are implemented. Four kinds of MA designs are selected and analyzed in this article by using the proposed methodology. Following are the solutions obtained for the considered MA designs.

1) Config-I^a: RBW$_{-10\,\text{dB}} =$ 5.47 GHz, and SWA $=$ 12.69 Np/m at $d = 5.6$ mm Ω, $Z_S = 301$, and $\varepsilon_r = 2.01$.
2) Config-II^a: RBW$_{-10\,\text{dB}} =$ 9.84 GHz, and SWA $=$ 6.85 Np/m at $d = d_1 + d_2 = 6.83$ mm, $Z_{S1} = 217.88\,\Omega$, $Z_{S2} = 608.73\,\Omega$, $\varepsilon_{r1} = 1.54$, and $\varepsilon_{r2} = 2.21$.
3) Config-I^b: RBW$_{-10\,\text{dB}} = 5.02$ GHz, and SWA $= 41$ Np/m at $\varepsilon_r = 2$, $d = 3$ mm, $R_s = 40\,\Omega$/Sq, $P = 10$ mm, and $w = 2.5$ mm.
4) Config-II^b: RBW$_{-10\,\text{dB}} = 9.4$ GHz, and SWA $= 40$ Np/m at $d = d_1 + d_2 = 4$ mm, $\varepsilon_{r1} = 2$, and $\varepsilon_{r2} = 1.7$, $R_{s1} = 40\,\Omega$/Sq, $R_{s2} = 10\,\Omega$/Sq, $P_1 = P_2 = 10$ mm, $w_1 = 1.5$ mm, and $w_2 = 3$ mm.

All the summarized solutions also meet the criteria of the RTL. Also, these solutions offer significant utility in situations where the requirement involves effectively managing both surface wave coupling and reducing the reflection coefficient within the same frequency range. We tested our proposed semianalytical 2D-DM method on four important structures in this manuscript and we believe that with a similar process as presented in this manuscript, other meta-material-based MA designs can also be analyzed to obtain desired solutions.

REFERENCES

[1] D. M. Pozar, *Microwave Engineering*, 3rd ed. Hoboken, NJ, USA: Wiley, 2005. [Online]. Available: https://cds.cern.ch/record/882338
[2] C. A. Balanis, *Advanced Engineering Electromagnetics*. New York, NY, USA: Wiley, 1989.
[3] C. Wang, E. Li, and D. F. Sievenpiper, "Surface-wave coupling and antenna properties in two dimensions," *IEEE Trans. Antennas Propag.*, vol. 65, no. 10, pp. 5052–5060, Oct. 2017.
[4] M. Alibakhshikenari, B. S. Virdee, C. H. See, R. A. Abd-Alhameed, F. Falcone, and E. Limiti, "Surface wave reduction in antenna arrays using metasurface inclusion for MIMO and SAR systems," *Radio Sci.*, vol. 54, no. 11, pp. 1067–1075, 2019.
[5] J.-G. Yook and L. Katehi, "Micromachined microstrip patch antenna with controlled mutual coupling and surface waves," *IEEE Trans. Antennas Propag.*, vol. 49, no. 9, pp. 1282–1289, Sep. 2001.
[6] M. Khayat, J. Williams, D. Jackson, and S. Long, "Mutual coupling between reduced surface-wave microstrip antennas," *IEEE Trans. Antennas Propag.*, vol. 48, no. 10, pp. 1581–1593, Oct. 2000.
[7] B.-I. Wu, H. Chen, J. A. Kong, and T. M. Grzegorczyk, "Surface wave suppression in antenna systems using magnetic metamaterial," *J. Appl. Phys.*, vol. 101, no. 11, 2007, Art. no. 114913.
[8] W. Emerson, "Electromagnetic wave absorbers and anechoic chambers through the years," *IEEE Trans. Antennas Propag.*, vol. 21, no. 4, pp. 484–490, Jul. 1973.
[9] K. J. Vinoy and K. M. Jha, *Radar Absorbing Materials*. Dodrecht, The Netherlands: Kluwer, 1996.
[10] F. Costa, A. Monorchio, and G. Manara, "Theory, design and perspectives of electromagnetic wave absorbers," *IEEE Electromagn. Compat. Mag.*, vol. 5, no. 2, pp. 67–74, Second Quarter 2016.

[11] V. Mishra, S. Puthucheri, and D. Singh, "Development of analytical approach to fabricate composites for microwave absorption," *IEEE Trans. Magn.*, vol. 53, no. 8, Aug. 2017, Art. no. 2800710.

[12] E. Michielssen, J.-M. Sajer, S. Ranjithan, and R. Mittra, "Design of lightweight, broad-band microwave absorbers using genetic algorithms," *IEEE Trans. Microw. Theory Techn.*, vol. 41, no. 6, pp. 1024–1031, Jun.–Jul. 1993.

[13] R. Fante and M. McCormack, "Reflection properties of the salisbury screen," *IEEE Trans. Antennas Propag.*, vol. 36, no. 10, pp. 1443–1454, Oct. 1988.

[14] B. Munk, *Frequency Selective Surfaces: Theory and Design*. Hoboken, NJ, USA: Wiley, 2005.

[15] A. Kazemzadeh and A. Karlsson, "Multilayered wideband absorbers for oblique angle of incidence," *IEEE Trans. Antennas Propag.*, vol. 58, no. 11, pp. 3637–3646, Nov. 2010.

[16] L. Li and Z. Lv, "Ultra-wideband polarization-insensitive and wide-angle thin absorber based on resistive metasurfaces with three resonant modes," *J. Appl. Phys.*, vol. 122, no. 5, 2017, Art. no. 055104, doi: 10.1063/1.4997468.

[17] Y.-Q. Pang, Y.-J. Zhou, and J. Wang, "Equivalent circuit method analysis of the influence of frequency selective surface resistance on the frequency response of metamaterial absorbers," *J. Appl. Phys.*, vol. 110, no. 2, 2011, Art. no. 023704, doi: 10.1063/1.3608169.

[18] F. Costa, A. Monorchio, and G. Manara, "An overview of equivalent circuit modeling techniques of frequency selective surfaces and metasurfaces," *Appl. Comput. Electromagnetics Soc. J.*, vol. 29, no. 12, pp. 960–976, Dec. 2014.

[19] X. Lv, S. J. Chen, A. Galehdar, W. Withayachumnankul, and C. Fumeaux, "Fast semi-analytical design for single-FSS-layer circuit-analog absorbers," *IEEE Open J. Antennas Propag.*, vol. 1, pp. 483–492, 2020.

[20] R. L. Haupt and D. H. Werner, *Genetic Algorithms in Electromagnetics*. Hoboken, NJ, USA: Wiley, 2007.

[21] B. Chambers, "Design of Wideband Jaumann radar absorbers with optimum oblique incidence performance," *Electron. Lett.*, vol. 30, no. 2, pp. 1530–1532, Sep. 1994.

[22] S. Genovesi, R. Mittra, A. Monorchio, and G. Manara, "Particle swarm optimization for the design of frequency selective surfaces," *IEEE Antennas Wireless Propag. Lett.*, vol. 5, pp. 277–279, 2006.

[23] S. K. Goudos and J. N. Sahalos, "Microwave absorber optimal design using multi-objective particle swarm optimization," *Microw. Opt. Technol. Lett.*, vol. 48, no. 8, pp. 1553–1558, 2006.

[24] E. Yigit and H. Duysak, "Determination of optimal layer sequence and thickness for broadband multilayer absorber design using double-stage artificial bee colony algorithm," *IEEE Trans. Microw. Theory Techn.*, vol. 67, no. 8, pp. 3306–3317, Aug. 2019.

[25] H. S. Farahani, M. Veysi, M. Kamyab, and A. Tadjalli, "Mutual coupling reduction in patch antenna arrays using a UC-EBG superstrate," *IEEE Antennas Wireless Propag. Lett.*, vol. 9, pp. 57–59, 2010.

[26] M. J. Al-Hasan, T. A. Denidni, and A. R. Sebak, "Millimeter-wave EBG-based aperture-coupled dielectric resonator antenna," *IEEE Trans. Antennas Propag.*, vol. 61, no. 8, pp. 4354–4357, Aug. 2013.

[27] M. J. Al Hasan, T. A. Denidni, and A. R. Sebak, "Millimeter-wave compact EBG structure for mutual coupling reduction applications," *IEEE Trans. Antennas Propag.*, vol. 63, no. 2, pp. 823–828, Feb. 2015.

[28] X. Tan, W. Wang, Y. Wu, Y. Liu, and A. A. Kishk, "Enhancing isolation in dual-band meander-line multiple antenna by employing split EBG structure," *IEEE Trans. Antennas Propag.*, vol. 67, no. 4, pp. 2769–2774, Apr. 2019.

[29] M. Neve and R. Paknys, "A technique for approximating the location of surface- and leaky-wave poles for a lossy dielectric slab," *IEEE Trans. Antennas Propag.*, vol. 54, no. 1, pp. 115–120, Jan. 2006.

[30] Y. Li, D. Li, H. Luo, F. Chen, X. Wang, and R. Gong, "Co-evaluation of reflection loss and surface wave attenuation for magnetic absorbing material," *IEEE Trans. Antennas Propag.*, vol. 66, no. 11, pp. 6057–6060, Nov. 2018.

[31] J. Richmond, L. Peters, and R. Hill, "Surface waves on a lossy planar ferrite slab," *IEEE Trans. Antennas Propag.*, vol. 35, no. 7, pp. 802–808, Jul. 1987.

[32] J. H. Richmond, "Propagation of surface waves on a thin resistive sheet or a coated substrate," *Radio Sci.*, vol. 22, no. 5, pp. 825–831, 1987.

[33] D. Shively, "Surface waves on a grounded dielectric slab covered by a resistive sheet," *IEEE Trans. Antennas Propag.*, vol. 41, no. 3, pp. 348–350, Mar. 1993.

[34] M. Zhang, L.-W. Li, and Y.-F. Tian, "An efficient approach for extracting poles of Green's functions in general multilayered media," *IEEE Trans. Antennas Propag.*, vol. 56, no. 1, pp. 269–273, Jan. 2008.

[35] D.-X. Wang, E. K.-N. Yung, R.-S. Chen, and J. Bao, "A new method for locating the poles of Green's functions in a lossless or lossy multilayered medium," *IEEE Trans. Antennas Propag.*, vol. 58, no. 7, pp. 2295–2300, Jul. 2010.

[36] J. Ding and S. L. Dvorak, "An accurate and systematic surface-wave pole location method for multilayered media," *IEEE Trans. Antennas Propag.*, vol. 62, no. 2, pp. 997–1001, Feb. 2014.

[37] V. Mishra, F. Costa, and A. Monorchio, "Surface wave attenuation in multilayer structures with lossy media and impedance surfaces," *IEEE Access*, vol. 9, pp. 130627–130637, 2021.

[38] V. Mishra, F. Costa, D. Brizi, and A. Monorchio, "Surface wave attenuation in salisbury screen in tm_0 mode," in *Proc. IEEE USNC-URSI Radio Sci. Meeting Joint With AP-S Symp.*, 2022, pp. 84–85.

[39] F. Costa, A. Monorchio, and G. Manara, "Efficient analysis of frequency-selective surfaces by a simple equivalent-circuit model," *IEEE Antennas Propag. Mag.*, vol. 54, no. 4, pp. 35–48, Aug. 2012.

[40] K. Rozanov, "Ultimate thickness to bandwidth ratio of radar absorbers," *IEEE Trans. Antennas Propag.*, vol. 48, no. 8, pp. 1230–1234, Aug. 2000.

Varsha Mishra (Member, IEEE) received the Ph.D. degree in electronics and communication engineering from the Indian Institute of Technology Roorkee, Roorkee, India, in 2019.

She has more than eight years of experience in working with sponsored projects related to the development of microwave absorbers for ICT solutions. From 2014 to 2019, she worked with Defence Research and Development Organization (DRDO) sponsored project on the development of experimental and analytical approaches for microwave absorbers. Since 2019, she has been working as a full-time Research Associate with the University of Pisa, Italy. The project is related to the development of meta-surfaces for ICT (information and communications technology) solutions. Her current research interests include developing electromagnetic techniques for microwave absorbers, meta-surfaces, electromagnetic interference, and guided EM wave propagation, measurement, EM wave exposure from cell phone, and human head modeling.

Dr. Mishra owns significant publications in well-reputed IEEE journals and international conferences, she is an author of Indian Patent. She serves as a Reviewer for renowned IEEE TEMC, IEEE AWPL, and Taylor & Francis journals.

Agostino Monorchio (Fellow, IEEE) received the Laurea degree in electronics engineering in 1991, and the Ph.D. degree in methods and technologies for environmental monitoring in 1994 from the University of Pisa, Pisa, Italy

He is currently a Full Professor of electromagnetic fields with University of Pisa. He has carried out a considerable research activity and technical consultancy to national, EU and U.S. industries, coordinating, as Principal scientific investigator, a large number of national and European research projects. He is active in a number of areas including computational electromagnetics, microwave metamaterials, radio propagation for wireless systems, the design and miniaturization of antennas and electromagnetic compatibility, and biomedical microwaves applications. His research results have been published in more than 170 journal papers and book chapters, and more than 260 communications at international and national conferences, he is the co-author of four patents. The activity is mainly carried out at the Microwave and Radiation Laboratory of the Department of Information Engineering, University of Pisa, together with a large group of Ph.D. students, Post-Docs, and Research Associates.

Mr. Monorchio is the Director of RaSS National Laboratory, Consorzio Nazionale Interuniversitario per le Telecomunicazioni. He is currently a Reviewer for international journals, and was an Associate Editor for IEEE ANTENNAS AND WIRELESS PROPAGATION LETTERS, from 2002 to 2007. He has been an AdCom member from 2017 to 2019, and is the co-chair of the Industrial Initiative Committee of the IEEE APS. He is a Member of the Scientific Advisory Board of Directed Energy Research Center of TII, Abu Dhabi, UAE, and affiliated with the Pisa Section of INFN, the National Institute of Nuclear Physics. He spent several research periods with the Electromagnetic Communication Laboratory, Pennsylvania State University, both as a recipient of a scholarship (Fellowship Award) of the Summa Foundation, New Mexico, and in the framework of CNR-NATO Senior Fellowship programme. In 2012, he has been elevated to Fellow grade by the IEEE for his contributions to computational electromagnetics and for application of frequency selective surfaces in metamaterials.